APL Materials ARTICLE scitation.org/journal/apm

Direct observation of mono-vacancy and self-interstitial recovery in tungsten

Cite as: APL Mater. 7, 021103 (2019); doi: 10.1063/1.5082150
Submitted: 19 November 2018 • Accepted: 3 February 2019 •
Published Online: 13 February 2019

J. Heikinheimo,[1] K. Mizohata,[2] J. Räisänen,[2] T. Ahlgren,[2] P. Jalkanen,[2] A. Lahtinen,[2] N. Catarino,[3] E. Alves,[3] and F. Tuomisto[1,a)]

AFFILIATIONS

[1]Department of Applied Physics, Aalto University, P.O. Box 15100, FI-00076 Aalto, Finland
[2]Department of Physics, University of Helsinki, P.O. Box 43, FI-00014 Helsinki, Finland
[3]IPFN, Instituto Superior Técnico, Universidade de Lisboa, 1049-001 Lisboa, Portugal

[a)]filip.tuomisto@aalto.fi

ABSTRACT

Reliable and accurate knowledge of the physical properties of elementary point defects is crucial for predictive modeling of the evolution of radiation damage in materials employed in harsh conditions. We have applied positron annihilation spectroscopy to directly detect mono-vacancy defects created in tungsten through particle irradiation at cryogenic temperatures, as well as their recovery kinetics. We find that efficient self-healing of the primary damage takes place through Frenkel pair recombination already at 35 K, in line with an upper bound of 0.1 eV for the migration barrier of self-interstitials. Further self-interstitial migration is observed above 50 K with activation energies in the range of 0.12–0.42 eV through the release of the self-interstitial atoms from impurities and structural defects and following recombination with mono-vacancies. Mono-vacancy migration is activated at around 550 K with a migration barrier of $E_m^V = 1.85 \pm 0.05$ eV.

Self-healing through migration and annihilation of lattice point defects determines the durability of a crystalline solid in heavy irradiation conditions.[1] Exposure to particle irradiation leads primarily to the formation of vacancy-type of defects and self-interstitial atoms (SIAs). With increasing particle flux, fluence, and time, these point defects migrate and eventually cluster, forming dislocation loops,[2,3] voids,[4] and stacking fault tetrahedra[5,6] in metals. Further growth of such defects leads to the appearance of features such as swelling, hardening, embrittlement, and direct failure. Full understanding of these phenomena and reliable prediction of material lifetime requires accurate knowledge of the radiation-induced creation and migration processes of the primary defects—mono-vacancies and SIAs—as well as the recombination rates of these defects.[7–9]

Tungsten (W), a metal with *bcc* lattice structure, is relied on as a plasma-facing material in ITER, one of the world's most ambitious energy projects.[10] The irradiation environment in the high-temperature fusion plasma is extremely hostile, eventually leading to the deterioration of thermal properties and loss of mechanical integrity of this so-called first wall. It is of paramount significance for the functioning of the reactor that this material preserves its structural integrity throughout its planned lifetime. Our ability to accurately and reliably determine the physical properties of radiation-induced defects currently limits the reliability of predictive modeling of the evolution of primary radiation damage.

A wide variety of methods has been employed to experimentally characterize early stage radiation damage recovery in tungsten, with the focus on SIA migration.[11] More recently, Amino *et al.* used high-voltage transmission electron microscopy to monitor low-temperature SIA dynamics.[12,13] These studies are based on the detection of large defect clusters, such as dislocation loops or macroscopic properties, since the ability of the applied methods to detect point-like

defects is limited. Irradiation damage phenomena in tungsten have been studied with positron annihilation spectroscopy but mainly from the point of view of hydrogen-vacancy and helium-vacancy interactions and high-temperature recovery processes.[14–17]

In this work, we apply positron annihilation spectroscopy to directly detect mono-vacancy defects created in tungsten through 10-MeV H^+ irradiation at 35 K. We analyze the recovery kinetics of these mono-vacancies and SIAs through post-irradiation thermal annealings up to 700 K. We find that the primary damage introduced at 35 K is efficiently reduced through Frenkel pair recombination, in line with the low migration barrier of the SIAs—recent defect clustering experiments[13] propose it to be less than 0.1 eV. In our experiments, we observe SIA migration above 50 K with activation energies in the range of 0.12–0.42 eV, and we interpret this to originate from the release of SIAs from impurities and structural defects. We observe the migration of mono-vacancies above 550 K and determine their migration barrier as $E_m^V = 1.85 \pm 0.05$ eV.

Positron annihilation spectroscopy allows non-destructive identification and quantification of atomic-sized open-volume defects in crystalline solids.[18] Thus the experimental approach adopted in this work is as follows. We apply our unique experimental setup[19] where 10-MeV proton irradiation was performed at 35 K with *in situ* positron lifetime measurements. High purity tungsten (99.95%, as rolled, thickness 50 μm, supplied by Goodfellow) with randomly oriented grains (average diameter of 250 nm) was employed. To induce recrystallization, the samples were annealed for 1 h at 1973 K in a vacuum of 5×10^{-4} Pa. The cooling rate after the annealing was roughly 300 K/min. During annealing, grain boundary movement took place, merging grains into larger ones with an average size of 25 μm. The samples were mounted in the conventional sandwich setup with a 1-MBq[22] NaCl e^+-source wrapped in a 3-μm Al foil, on an aluminum sample holder in thermal contact with a closed-cycle helium cryostat. For the positron lifetime analysis, we used a fast digital spectrometer[20] with a resolution of 260 ps. The average positron implantation depth in W is approximately 15 μm, and the projected range of 10 MeV protons in W is approximately 170 μm. Hence we avoid end-of-range effects in the positron experiments. Approximately 10^6 counts were collected for each lifetime spectrum, and the corrections for annihilations in the source were determined as 15.7% (210 ps) and 6.0% (400 ps).

The irradiations of the whole sample-source-sample sandwich were performed at 35 K in three stages, starting from a fluence of 1×10^{14} cm^{-2} up to 1×10^{16} cm^{-2}, to monitor the defect production. The current density was kept low, below 100 nA/cm^2, to avoid local heating effects during the irradiation. After the highest-fluence irradiation, the samples were annealed for 1 h with 10 K steps up to room temperature (RT) and the positron lifetime was measured at 35 K between the annealing steps. After reaching RT, the positron lifetime was measured as a function of temperature in the range 35–300 K. Finally, the sample-source-sandwich was removed from the cryostat; thermal annealings were continued with 20 K steps (1 h) up to 700 K; and the positron lifetime was measured at RT between the annealing steps. The experimental positron lifetime spectra were analyzed as the sum of exponential decay components convoluted with the Gaussian resolution function of the spectrometer after subtracting the constant background and annihilations in the source material. Each positron state in the matter gives a characteristic lifetime $\tau_i = 1/\lambda_i$, where λ_i is the annihilation rate associated with the positron state. The increase in the average lifetime τ_{ave} above the bulk lattice lifetime τ_B shows that vacancy defects are detected in the sample. The average lifetime that coincides with the center of mass of the lifetime spectrum is statistically very accurate, enabling reliable detection of spectral changes.

Figure 1 shows the average positron lifetime τ_{ave} measured at 35 K as a function of annealing temperature in the irradiated tungsten sample. For reference, we measured several well-annealed high-purity single crystal W samples that produced a lifetime spectrum with only one component that can be associated with the W lattice: τ_B = 110–112 ps. As the figure shows, 10-MeV proton irradiation to fluences 10^{14}–10^{15} cm^{-2} produced only modest changes to the average positron lifetime, from τ_{ave} = 112 ps to τ_{ave} = 115 ps. The annealing experiments were stopped around 150 K for these irradiations. Only the irradiation to a fluence 1×10^{16} cm^{-2} produced a significant increase, and the recovery of the irradiation damage is clearly visible starting at around 50 K. Two lifetime components were separable in the spectra, giving $\tau_2 = 180 \pm 15$ ps for the second (longer) component. Interestingly, the first lifetime component τ_1 is also rather constant and slightly longer than τ_B, in the 112–120 ps range. The decrease in τ_{ave} at annealing temperatures 50–130 K is evidently due to the decrease in the intensity I_2 of the second lifetime component τ_2.

The as-received polycrystalline W sample gave τ_{ave} = 112 ps when measured at 35 K, but at RT, the average lifetime was significantly longer, τ_{ave} = 118 ps. Typically, thermal expansion of the crystalline lattice produces changes[21] of at most 0.2–1 ps/100 K in τ_{ave}. Hence, in order to check whether the positron annihilation data measured in the irradiated sample are affected by temperature-dependent positron trapping phenomena, we performed the positron lifetime experiments as a function of measurement temperature after the thermal recovery of the 1×10^{16} cm^{-2} irradiated sample up to RT. The behavior of the average lifetime in Fig. 2 shows very clear temperature dependence, with almost 20 ps difference between 35 K and RT. The two-component decomposition of the lifetime spectra gives a second lifetime component of $\tau_2 = 180 \pm 15$ ps as in the annealing experiment, but with significant scatter and larger statistical uncertainties in the fitting at low temperatures. Similar scatter is in fact observed in the annealing data at 200-300 K in Fig. 1, and it is due to the rather low intensity I_2 (in the data of Fig. 2, I_2 is in the range of 30%-40% above 150 K and reduces to less than 10% at low temperatures). The shorter lifetime component τ_1 is in the range 110-125 ps throughout the measurement temperature range.

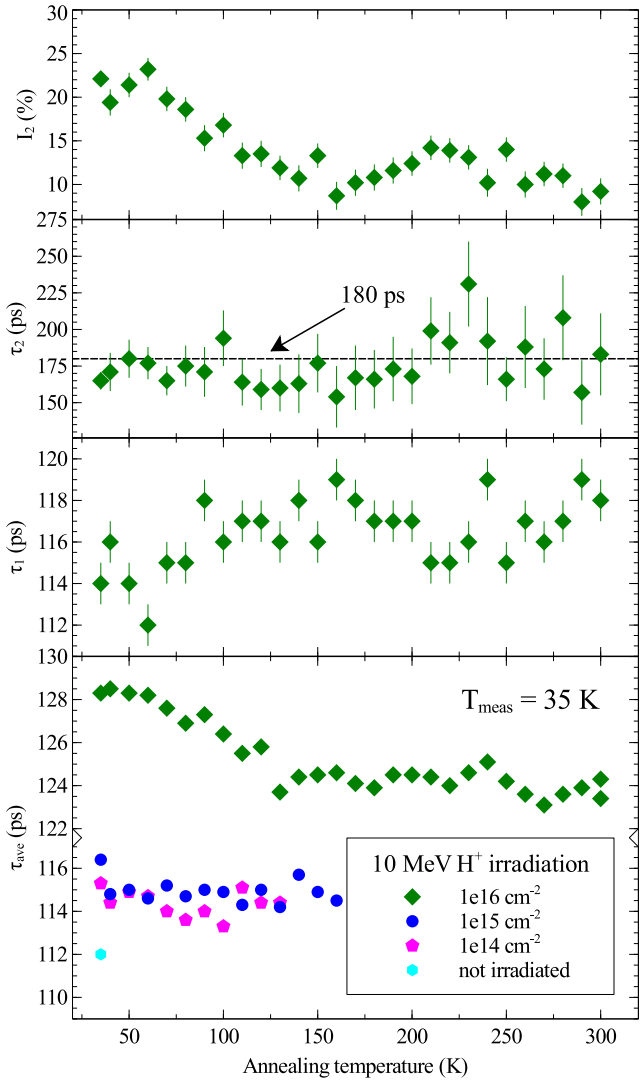

FIG. 1. Average positron lifetime as a function of annealing temperature in irradiated W. Measurements were performed at 35 K. The upper panels show the two lifetime components τ_1 and τ_2 separated from the lifetime spectra, as well as the intensity I_2 of the second lifetime component. The recovery of the irradiation damage is clearly visible, starting at around 50 K.

Our previous work has shown that the 10-MeV proton irradiation at low temperatures leads to mono-vacancy formation.[19,22,23] Hence we identify the second lifetime component $\tau_2 = 180 \pm 15$ ps observed in the irradiated tungsten samples as originating from mono-vacancies. This finding is consistent with earlier positron annihilation experiments and theoretical calculations that have attributed lifetimes in the range 160–200 ps to the W mono-vacancy.[15,24–26] To quantify the mono-vacancy production in the irradiation and to analyze the damage recovery in detail, we first need to consider the implications of the temperature dependence of $\tau_{ave} = 118$ in Fig. 2.

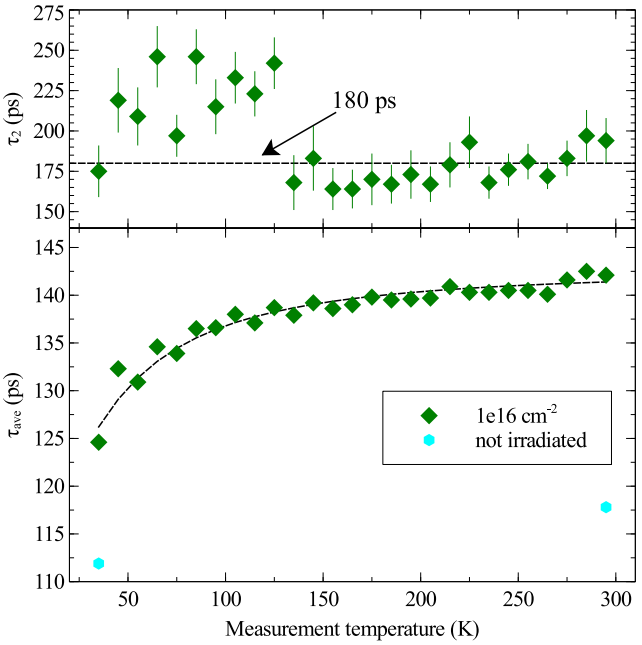

FIG. 2. Temperature behavior of the average positron lifetime τ_{ave} in the irradiated sample after annealing at RT. The upper panel shows the second lifetime component τ_2. The temperature behavior of these data suggests that structural defects such as dislocations and grain boundaries compete with vacancy defects in positron trapping at low temperatures. The solid curve shows the best fit of the two-defect model described in the text.

The fact that $\tau_1 > \tau_B$ in all the experiments implies that positrons are trapped at other defects than mono-vacancies in the irradiated samples, with a defect-related lifetime close to that of the W lattice. The temperature dependence of τ_{ave} in both the as-received and irradiated polycrystalline W samples (at RT $\tau_{ave} > \tau_B$ also in the as-received sample) indicates that the trapping of positrons to these defects is strongly enhanced at low temperatures. This suggests that the trapping is diffusion limited to the defects in question. With the short lifetime, this makes structural defects such as dislocations and grain boundaries the most likely cause for the observed positron trapping.

In the presence of two kinds of defects (D1 and D2) that act as positron traps, the average positron lifetime is written as

$$\tau_{ave} = \frac{\lambda_B\tau_B + \kappa_{D1}\tau_{D1} + \kappa_{D2}\tau_{D2}}{\lambda_B + \kappa_{D1} + \kappa_{D2}}, \quad (1)$$

where $\lambda_B = \tau_B^{-1}$ is the bulk annihilation rate, κ_i is the trapping rate to defect i, and τ_i is the lifetime related to defect i. The trapping rate to a defect is proportional to its concentration (c_i): $\kappa_i = \mu_i c_i$, where the proportionality factor μ_i is called the trapping coefficient. For mono-vacancies in body centered cubic transition metals, $\mu_V \approx 10^{15}$ s^{-1},[27] and it is temperature-independent. However, if positron trapping is limited by diffusion (and hence scattering off, e.g., phonons), the trapping coefficient behaves as T^{-n}, with experimentally observed values of n ranging from 0.5 to 1.5.[28]

We can fit the temperature-dependent τ_{ave} data in Fig. 2 with Eq. (1) using τ_{D2} = 180 ps for mono-vacancies, τ_{D1} = 110–120 ps for the structural defects, and τ_B = 100–110 ps for the annihilations in the bulk. In addition, the trapping rate to the mono-vacancies is kept constant as a function of temperature. The best fit (shown in the figure) is obtained by assuming τ_B = 100 ps, τ_{D1} = 112 ps, and a $T^{-1.5}$ temperature dependence for the structural defects. We obtain $\kappa_{D2} \simeq \lambda_B$ and $\kappa_{D1}(T = 35\ K) \simeq 3\lambda_B$. At RT, $\kappa_{D2} \gg \kappa_{D1} \simeq 0.1\lambda_B$, making positron trapping at the structural defects a negligible effect at RT. The magnitude and temperature dependence of κ_{D1} also explain the temperature behavior of τ_{ave} in the as-received W, with an effective $\kappa^*_{D2} \simeq 0.3\lambda_B$. In addition, the effect of the lower-fluence irradiations (see Fig. 1) is consistent with these numbers. Hence, the structural defects (collectively called D1) are not modified by the irradiation and the following thermal annealing below RT and can be assumed to affect all the results of the low-temperature measurements in the same way. It should be noted that the vacancy defects in the as-received samples are probably not mono-vacancies, but since they cannot be resolved, we make this simplification in the further analysis to better estimate the mono-vacancy introduction rate in the irradiation.

With the knowledge $\kappa_{D1}(T = 35\ K)$, we can solve κ_{D2} from Eq. (1) for each annealing temperature from the lifetime data shown in Fig. 1, giving

$$\kappa_{D2} = \frac{\tau_{ave} - \tau_B}{\tau_{D2} - \tau_{ave}}\lambda_B - \frac{\tau_{D1} - \tau_{ave}}{\tau_{D2} - \tau_{ave}}\kappa_{D1}(T = 35\ K). \quad (2)$$

The trapping rate associated with the irradiation-induced mono-vacancies is finally estimated as $\kappa_V = \kappa_{D2} - \kappa^*_{D2}$ and shown as a function of annealing temperature in Fig. 3. The

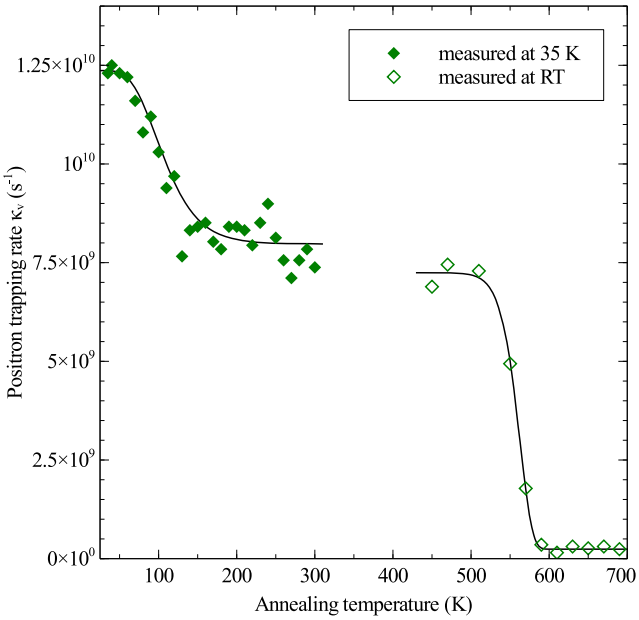

FIG. 3. Positron trapping rate to mono-vacancies in tungsten. The curves are fitted based on the model describing the isochronal annealing process.

above-RT annealing τ_{ave} data are much more straightforward to analyze since the contribution of the structural defects (D1) can be neglected, eliminating the second term from the right-hand-side of Eq. (2). As the trapping rate is proportional to the concentration of the irradiation-induced mono-vacancies, we can fit the activation energy E_A for their removal similarly as in Ref. 23. The isochronal annealing process for a defect concentration N can be described as

$$N_{i+1} = N_\infty + (N_i - N_\infty)\exp(-\nu t \cdot \exp(-E_A/(kT_i))), \quad (3)$$

where the subscript i denotes the annealing step, t = 3600 s is the annealing time, and $\nu = 10^{13}\ s^{-1}$ is an estimated frequency factor.[29]

Using this model, an activation energy of E_A = 1.85 ± 0.05 eV can be fitted to the annealing stage observed at T = 550 K. In earlier experiments, the mono-vacancy migration barrier has been determined as 1.78 ± 0.1 eV,[30] while theoretical predictions for mono-vacancy migration barriers are in the range 1.4–1.8 eV.[31–33] These are in agreement with our value, and hence we identify this activation energy as the mono-vacancy migration barrier, E^V_m = 1.85 ± 0.05 eV, found through direct observation of the recovery of irradiation-induced mono-vacancies. The low-temperature annealing stage at 50–130 K could not be fitted with single activation energy. Instead a linear dependence $E_A = E_0 + \alpha(T_i - T_1)$ was assumed. The fitting gave activation energies ranging from 0.12 ± 0.01 eV at the beginning of the stage at 50 K to 0.42 ± 0.01 eV at the end at about 130 K. This kind of "sliding" of the activation energy can be expected if the migrating defects are not all identical and have different diffusion barriers, leading to a complex annealing behavior. Earlier experimental and theoretical work suggests that the SIA migration barrier is well below 0.1 eV.[12,13,31–34] However, in poly-crystalline tungsten, the SIAs may be trapped by structural defects and by impurities. The dissociation energy of SIA from hydrogen has been predicted as 0.43 eV,[32] similar to the activation energy fitted above. Hence we interpret the first recovery stage observed in our experiments as SIAs being released from their traps and recombining with mono-vacancies. Roughly 40% of the irradiation-induced mono-vacancies are annealed out in the first stage through the SIA migration and the rest through mono-vacancy migration.

The introduction rate of the mono-vacancies in the 10-MeV proton irradiation (fluence $1 \times 10^{16}\ cm^{-2}$) at 35 K can be estimated from the trapping rate $\kappa_V \simeq 1.25 \times 10^{10}\ s^{-1}$ using the trapping coefficient $\mu_V = 10^{15}\ s^{-1}$ and the W atomic density $N_{at} = 6.4 \times 10^{22}\ cm^{-3}$. The density of the introduced mono-vacancies is $[V] \simeq 8 \times 10^{17}\ cm^{-3}$, giving an introduction rate $\Sigma_V \simeq 80\ cm^{-1}$. This value should be compared with the primary defect production rates that can be calculated, for example, with the McKinley-Feshbach relativistic displacement cross-sectional formula.[29] Using an average threshold displacement energy[35] of 55–60 eV and averaging over 3–10 MeV to mimic the range of irradiation damage probed by the positrons, the introduction rate is obtained as $\Sigma_V^{theory} \simeq 400\ cm^{-1}$. SRIM simulations[36] give somewhat higher values, $\Sigma_V^{SRIM} = 800 - 1000\ cm^{-1}$, along the ion range probed by

positrons. The difference in the experimental and simulated values suggests that a significant part of the radiation damage is already self-healed at the very low irradiation temperature of 35 K. This means that SIAs already recombine with mono-vacancies very efficiently during the irradiation process, placing an upper bound on the migration barrier as $E_m^{SIA} < 0.1$ eV.

In summary, we have made direct observations of SIA and mono-vacancy migration phenomena in tungsten. Applying positron lifetime spectroscopy *in situ* with ion irradiation at cryogenic temperatures allowed us to perform fast and accurate measurements of the migration barriers. We first observe that the mono-vacancy introduction rate is significantly lower than that expected for primary damage and interpret this as evidence of efficient dynamic Frenkel pair recombination. This places an upper bound on the SIA migration barrier as $E_m^{SIA} < 0.1$ eV, in line with the recent defect clustering experiments.[13] Then, at 50 K, we observe the onset of SIA migration through their release from impurities and structural defects, with activation energies in the range of 0.12–0.42 eV. Finally, around 550 K, mono-vacancy migration is activated with a migration barrier of $E_m^V = 1.85 \pm 0.05$ eV.

This project was partially funded by the Academy of Finland Project No. 277193 and by the Finnish Center of Excellence in Atomic Layer Deposition.

REFERENCES

[1] G. Ackland, Science **327**, 1587–1588 (2010).
[2] K. Arakawa, K. Ono, M. Isshiki, K. Mimura, M. Uchikoshi, and H. Mori, Science **318**, 956–959 (2007).
[3] S. V. Starikov, Z. Insepov, J. Rest, A. Y. Kuksin, G. E. Norman, V. V. Stegailov, and A. V. Yanilkin, Phys. Rev. B **84**, 104109 (2011).
[4] W. Xu, Y. Zhang, G. Cheng, W. Jian, P. C. Millett, C. C. Koch, S. N. Mathaudhu, and Y. Zhu, Nat. Commun. **4**, 2288 (2013).
[5] K. Nordlund and F. Gao, Appl. Phys. Lett. **74**, 2720–2722 (1999).
[6] M. Loretto, P. Phillips, and M. Mills, Scr. Mater. **94**, 1–4 (2015).
[7] F. Granberg, K. Nordlund, M. W. Ullah, K. Jin, C. Lu, H. Bei, L. M. Wang, F. Djurabekova, W. J. Weber, and Y. Zhang, Phys. Rev. Lett. **116**, 135504 (2016).
[8] A. Boulle and A. Debelle, Phys. Rev. Lett. **116**, 245501 (2016).
[9] F. X. Zhang, S. Zhao, K. Jin, H. Xue, G. Velisa, H. Bei, R. Huang, J. Y. P. Ko, D. C. Pagan, J. C. Neuefeind, W. J. Weber, and Y. Zhang, Phys. Rev. Lett. **118**, 205501 (2017).
[10] J. Roth, E. Tsitrone, A. Loarte, T. Loarer, G. Counsell, R. Neu, V. Philipps, S. Brezinsek, M. Lehnen, P. Coad, C. Grisolia, K. Schmid, K. Krieger, A. Kallenbach, B. Lipschultz, R. Doerner, R. Causey, V. Alimov, W. Shu, O. Ogorodnikova, A. Kirschner, G. Federici, and A. Kukushkin, J. Nucl. Mater. **390–391**, 1 (2009).
[11] F. Maury, M. Biget, P. Vajda, A. Lucasson, and P. Lucasson, Radiat. Eff. **38**, 53–65 (1978).
[12] T. Amino, K. Arakawa, and H. Mori, Philos. Mag. Lett. **91**, 86 (2011).
[13] T. Amino, K. Arakawa, and H. Mori, Sci. Rep. **6**, 26099 (2016).
[14] A. Debelle, M. F. Barthe, and T. Sauvage, J. Nucl. Mater. **376**, 216 (2008).
[15] P. E. Lhuillier, M. F. Barthe, P. Desgardin, W. Egger, and P. Sperr, Phys. Status Solidi C **6**, 2329–2332 (2009).
[16] P. E. Lhuillier, T. Belhabib, P. Desgardin, B. Courtois, T. Sauvage, M. F. Barthe, A. L. Thomann, P. Brault, and Y. Tessier, J. Nucl. Mater. **433**, 305 (2013).
[17] C. N. Taylor, M. Shimada, B. J. Merrill, D. W. Akers, and Y. Hatano, J. Nucl. Mater. **463**, 1009 (2015).
[18] F. Tuomisto and I. Makkonen, Rev. Mod. Phys. **85**, 1583–1631 (2013).
[19] S. Väyrynen, P. Pusa, P. Sane, P. Tikkanen, J. Räisänen, K. Kuitunen, F. Tuomisto, J. Härkönen, I. Kassamakov, E. Tuominen, and E. Tuovinen, Nucl. Instrum. Methods Phys. Res., Sect. A **572**, 978 (2007).
[20] J. Nissilä, K. Rytsölä, R. Aavikko, A. Laakso, K. Saarinen, and P. Hautojärvi, Nucl. Instrum. Methods Phys. Res., Sect. A **538**, 778 (2005).
[21] C. Le Berre, C. Corbel, K. Saarinen, S. Kuisma, P. Hautojärvi, and R. Fornari, Phys. Rev. B **52**, 8112 (1995).
[22] J. Slotte, S. Kilpeläinen, F. Tuomisto, J. Räisänen, and A. N. Larsen, Phys. Rev. B **83**, 235212 (2011).
[23] N. Segercrantz, J. Slotte, F. Tuomisto, K. Mizohata, and J. Räisänen, Phys. Rev. B **95**, 184103 (2017).
[24] M. J. Puska, M. Sob, G. Brauer, and T. Korhonen, J. Phys. IV France **05**, C1-135–C1-142 (1995).
[25] P. M. G. Nambissan and P. Sen, Radiat. Eff. Defects Solids **124**, 215–221 (1992).
[26] T. Troev, E. Popov, P. Staikov, N. Nankov, and T. Yoshiie, Nucl. Instrum. Methods Phys. Res., Sect. B **267**, 535–541 (2009).
[27] A. Dupasquier and A. P. Mills, Jr., *Positron Spectroscopy of Solids* (IOS Press, 1995).
[28] K. Saarinen, P. Hautojärvi, and C. Corbel, in *Identification of Defects in Semiconductors*, edited by M. Stavola (Academic Press, New York, 1998), p. 209.
[29] F. Agulló-López, C. R. A. Catlow, and P. D. Townsend, *Point Defects in Materials* (Academic Press, 1988).
[30] K.-D. Rasch, R. W. Siegel, and H. Schultz, Philos. Mag. A **41**, 91 (1980).
[31] L.-L. Niu, Y. Zhang, X. Shu, S. Jin, H.-B. Zhou, F. Gao, and G.-H. Lu, J. Phys.: Condens. Matter **27**, 255007 (2015).
[32] K. Heinola, T. Ahlgren, K. Nordlund, and J. Keinonen, Phys. Rev. B **82**, 094102 (2010).
[33] D. Nguyen-Manh, A. P. Horsfield, and S. L. Dudarev, Phys. Rev. B **73**, 020101 (2006).
[34] S. P. Fitzgerald and D. Nguyen-Manh, Phys. Rev. Lett. **101**, 115504 (2008).
[35] D. R. Mason, X. Yi, M. A. Kirk, and S. L. Dudarev, J. Phys.: Condens. Matter **26**, 375701 (2014).
[36] J. F. Ziegler, M. D. Ziegler, and J. P. Biersack, Nucl. Instrum. Methods Phys. Res., Sect. B **268**, 1818–1823 (2010).